



HAL
open science

Coiled-coil oligomerization controls localization of the plasma membrane REMORINs

Denis Martinez, Anthony Legrand, Julien Gronnier, Marion Decossas, Paul Gouguet, Olivier Lambert, Melanie Berbon, Loris Verron, Axelle Grelard, Veronique Germain, et al.

► To cite this version:

Denis Martinez, Anthony Legrand, Julien Gronnier, Marion Decossas, Paul Gouguet, et al.. Coiled-coil oligomerization controls localization of the plasma membrane REMORINs. *Journal of Structural Biology*, In press, 206 (1), pp.12-19. 10.1016/j.jsb.2018.02.003 . hal-02536974

HAL Id: hal-02536974

<https://hal.science/hal-02536974>

Submitted on 22 Oct 2021

HAL is a multi-disciplinary open access archive for the deposit and dissemination of scientific research documents, whether they are published or not. The documents may come from teaching and research institutions in France or abroad, or from public or private research centers.

L'archive ouverte pluridisciplinaire **HAL**, est destinée au dépôt et à la diffusion de documents scientifiques de niveau recherche, publiés ou non, émanant des établissements d'enseignement et de recherche français ou étrangers, des laboratoires publics ou privés.



Distributed under a Creative Commons Attribution - NonCommercial 4.0 International License

Coiled-coil oligomerization controls nanodomain organization of the plasma membrane REMORINs.

Denis Martinez^a, Anthony Legrand^a, Julien Gronnier^{b#}, Marion Decossas^c, Paul Gouguet^b, Olivier Lambert^c, Mélanie Berbon^a, Loris Verron^a, Axelle Grélard^a, Veronique Germain^b, Antoine Loquet^{a*}, Sébastien Mongrand^{b*}, Birgit Habenstein^{a*}

^a Institute of Chemistry & Biology of Membranes & Nanoobjects (UMR5248 CBMN),

sebastien.mongrand@u-bordeaux.fr (S. Mongrand) and b.habenstein@iecb.u-bordeaux.fr (B. Habenstein)

Abstract:

REMORINs are nanodomain-organized proteins located in the plasma membrane

structural mechanisms of REMORIN trimerization. Our results suggest that the formation of REMORIN coiled-coil trimers is essential for membrane recruitment and promotes REMORIN assembly *in vitro* into long filaments by trimer-trimer interactions that might participate in nanoclustering into membrane domains *in vivo*.

Keywords:

REMORIN

Nanodomain

Membrane protein

Solid-state NMR

Protein filament

Introduction

Membrane nanodomains are dynamic cellular signalling platforms in the plasma membrane of a size of up to a several hundred nanometers that execute essential messaging events between cells and their surroundings (Lingwood and Simons, 2010). Selective dynamic recruitment of specific proteins mediates the formation of functional membrane sub-compartments, related to signal transduction (Grecco et al., 2011) and membrane trafficking (Simons and Sampaio, 2011). Clustering of proteins into membrane compartments is notably driven by protein-lipid and protein-protein interactions (Lingwood and Simons, 2010). A significant number of membrane proteins are involved in protein-protein interactions leading to homo- or hetero-oligomers (McBride et al., 2017). Protein homo- or hetero-oligomerization has been proposed to mediate protein clustering (Kasai and Kusumi, 2014; Suzuki et al., 2012). Moreover, specific nanoclustering of proteins can drive functional compartmentalization, i.e. distinct nanodomains can be enriched in distinct nanodomain-associated proteins (Bucherl et al., 2017; Jarsch et al., 2014). As a consequence of the complexity of the system, i.e. proteins associated to membrane domains, insights into the structural and mechanistic organization of these proteins are sparse.

The REMORIN family consists of six phylogenetically distinguishable groups (Raffaele et al., 2007) of plant-specific nanodomain-organized proteins of the inner-leaflet of the plasma membrane (PM). Members of the REMORIN family carry out multiple functions related to biotic and abiotic stimuli (Jarsch and Ott, 2011; Lefebvre et al., 2010; Raffaele et al., 2009; Gui et al., 2014). In contrast to a highly variable N-terminal region, putatively implicated in protein-protein interactions (Marin et al., 2012; Toth et al., 2012), all REMORINs contain a conserved C-terminal region that encompasses a predicted coiled-coil domain (Bariola et al., 2004; Raffaele et al., 2007; Reymond et al., 1996), as well as a short membrane anchor domain (Gronnier et al., 2017; Perraki et al., 2012).

Coiled-coil domains are frequent motifs observed in proteins promoting multimerization towards homo- and also hetero-oligomers (Crick, 1953; Kohn et al., 1997; Lupas and Bassler, 2017). Proteins of the REMORIN family can oligomerize *in vivo* and *in vitro* into a filamentous state, possibly mediated by the coiled-coil domain (Bariola et al., 2004; Perraki et al., 2012). The *in vivo* functions of REMORIN oligomerization are not understood but they might include protein clustering to assure the nanodomain-mediated tasks. Nanoclustering of proteins is proposed to play an essential role in the segregation and functionalization of membrane rafts (Simons and Sampaio, 2011). Subtype Group 1 REMORINs form trimeric coiled-coil superstructures *in vitro* (Perraki et al., 2012) that lead to the formation of filamentous complexes (Bariola et al., 2004).

Our studies on the membrane anchoring mechanism and nanodomain targeting have recently revealed unconventional protein-membrane interactions mediated by the last 28 residues of the C-terminal region (REMORIN C-terminal anchor, REMCA) (Gronnier et al., 2017) that anchors to the surface of the plasma membrane without providing any transmembrane segment. The role of REMORIN oligomerization during this process remains obscure.

Magic-angle-spinning (MAS) solid-state nuclear magnetic resonance (SSNMR) and cryo-electron microscopy (cryo-EM) are both powerful emerging techniques useful to investigate assembled biomolecules in their native states. These techniques have the complementary characteristics of providing atomic data (reviewed for example in (Habenstein and Loquet, 2015; Loquet et al., 2013; Meier and Bockmann, 2015;

Tycko and Wickner, 2013; Weingarh and Baldus, 2013)) and detailed shape / symmetry information (reviewed for example in (Bai et al., 2015; Earl et al., 2017; Jiang and Tang, 2017; Vonck and Mills, 2017)), respectively.

We have here taken advantage of several biochemical, biophysical and bioinformatic tools to decipher the role and the structure of REMORINs' assembly. We report that multimerization of REMORINs into trimers confers their membrane affinity and could participate in the nanoclustering into membrane domains. Establishing homogeneous filament formation of the protein core involved in oligomerization allowed us to combine SSNMR and cryo-EM to gain insights into the supramolecular architecture of oligomerized REMORIN filaments.

We can thus add another piece to the puzzle of the unconventional mechanism of membrane binding and nanodomain recruitment of the REMORIN family. The coiled-coil superstructures of the REMORINs hold functions resulting from the assembled complexes rather than from their monomeric subunits.

Material and Methods

Expression, purification and filament formation of recombinant StREM1.3₈₆₋₁₉₈

E. coli BL21 (DE3) strains were transformed with a pET24-StREM1.3(86-198)-His₆ vector, containing the DNA encoding for residues 86-198 of REMORIN1.3 of *Solanum tuberosum*, and plated onto LB agar plates containing 30 mg/mL kanamycin. A flask containing 10 mL of LB medium was inoculated with a single colony and incubated overnight at 37°C under shaking at 200 rpm. The culture and expression of uniformly labelled ¹⁵N,¹³C StREM1.3(86-198)-His₆ (hereafter called REM_{H6(86-198)}) was performed in M9 medium supplemented in ¹⁵NH₄Cl and ¹³C₆-D-glucose as nitrogen and carbon sources. The labelled M9 medium was inoculated with 2% (v/v) of the unlabelled LB preculture and incubated at 37°C under shaking until the OD₆₀₀ reaches 0.7-0.8. At this stage, 1 mM IPTG was added to the culture for 20h protein expression at 18°C. Cells are then harvested by centrifugation (6000 g, 10 min, 4°C) and resuspended in the lysis buffer (20 mM HEPES, 150 mM NaCl, 20 mM imidazole, 1 mM PMSF, 1 tablet of Complete (Roche), 0.02 % NaN₃, pH 7.4). Cells were lysed by sonication on ice for 3 minutes, 30% magnitude (30 sec pulses,

30 sec intervals). The suspension was centrifuged at 15 000 g for 15 min at 4°C to recover the supernatant. The affinity purification was realised with the Äkta Pure 25 HPLC system (GE Healthcare Life Sciences) using a His-trap HP affinity column equilibrated with 5 column volumes of washing buffer (20 mM HEPES, 150 mM NaCl, 20 mM imidazole, 0.02 % NaN₃, pH 7.4). The protein was eluted with a linear gradient from 0 to 100 % of elution buffer (20 mM HEPES, 150 mM NaCl, 500 mM imidazole, 0.02 % NaN₃, pH 7.4) which led to a final yield of 10 mg of pure ¹⁵N, ¹³C labeled protein per liter of culture (Figure S1). Protein filaments were obtained by dialyzing overnight at room temperature the eluted sample against the assembly buffer (10 mM HEPES, 50 mM NaCl, 0.02 % NaN₃, pH 7.4). Protein filaments of REM₍₈₆₋₁₉₈₎, *i.e.* REM_{H6(86-198)} lacking the N-terminal His₆-tag, were prepared as follows. Affinity purification was performed as described above using a different washing buffer (50 mM Tris, 100 mM NaCl, 0.5 mM EDTA, 1 mM DTT, 0.5 mM PMSF, 0.02% NaN₃, pH=8.1) and elution buffer (50 mM Tris, 100 mM NaCl, 0.5 mM EDTA, 1 mM DTT, 0.5 mM PMSF, 500 mM imidazole, 0.02% NaN₃, pH=8.1). REM_{H6(86-198)} contains a TEV cleavable His₆-tag at its N-terminus. Eluted proteins and the TEV protease were mixed in a 100:1 (w/w) ratio, incubated at 4°C overnight under shaking and dialyzed against 1L of assembly buffer as described above to obtain REM₍₈₆₋₁₉₈₎ filaments.

For ssNMR studies, filaments of REM₍₈₆₋₁₉₈₎ lacking the N-terminal His₆-tag were prepared with a different protocol to enhance purity / yield of the sample. Expression and affinity purification was performed as described for filaments of uniformly ¹⁵N, ¹³C-labelled REM_{H6(86-198)}. Eluted protein fractions were pooled and adjusted to 0.5 mM EDTA and 1 mM DTT. Eluted proteins and TEV protease were mixed in a 100:1 (w/w) ratio, incubated at room temperature for 3h under shaking and dialyzed overnight at 4°C against the following buffer: 20 mM HEPES, 150 mM NaCl, 0.02% NaN₃, pH=7.4. After dialysis, urea was added to the proteins up to 7 M urea and REM₍₈₆₋₁₉₈₎ was retrieved on a His-trap HP column with the following washing buffer: 20 mM HEPES 150 mM NaCl 7 M urea pH=7.4; and elution buffer: 20 mM HEPES, 150 mM NaCl, 7 M urea, 500 mM imidazole, pH=7.4. REM₍₈₆₋₁₉₈₎ was enriched in the flowthrough. Uncleaved REM_{H6(86-198)} and TEV protease, containing a His₆-tag, bound to the column and were then eluted. Fractions containing REM₍₈₆₋₁₉₈₎ were pooled and

concentrated in an Amicon Ultra-15 centrifugal filter unit with MWCO = 3 kDa up to 0.8 mM, then dialyzed at room temperature against the assembly buffer (10 mM HEPES, 50 mM NaCl, 0.02% NaN₃, pH=7.4). The sample was then incubated at 37°C for 3h under shaking then at room temperature for 7 days.

Coiled-coil prediction and sequence alignment

StREM1.3₍₈₆₋₁₉₈₎ coiled-coil domain was identified using the software COILS (Lupas et al., 1991) and helical wheel diagrams for coiled-coils were built with DrawCoil 1.0 (<http://www.grigoryanlab.org/drawcoil/>).

Arabidopsis REMORINs were retrieved from (Raffaele et al., 2007). Protein alignment was computed using MULTiple Sequence Comparison by Log-Expectation (MUSCLE; (Edgar, 2004)) using BLOSUM62 matrix, an -sv profile scoring method with following parameters; Anchor spacing:32, diagonal break:1, diagonal length:24, diagonal margin:5, gap extension penalty:-1, gap open penalty:-12, hydro:5 and hydro factor1.2) through the JABAWS server (Troshin et al., 2011). Sequence alignments were rendered via the Jalview plugin (Waterhouse et al., 2009) (Figure S2).

Microsomal purification and Western blot analyses

Microsomal and soluble fractions from *Nicotiana benthamiana* leaves expressing GFP-StREM1.3 constructs were prepared as described in Perraki et al., 2012. Each fraction was analyzed by western blot using antibodies against StREM1.3 (Raffaele et al., 2009).

In vivo confocal imaging

Live cell imaging was performed using a Leica SP5 confocal laser scanning microscopy system (Leica, Wetzlar, Germany) equipped with Argon, DPSS and He-Ne lasers and hybrid detectors. Two days after agro-infiltration *N. benthamiana* leaves samples were transferred between a glass slide and a cover slip in a drop of water. GFP fluorescence was observed with excitation wavelengths of 488 nm and emission wavelengths of 490 to 550 nm. Experiments were performed using strictly identical confocal acquisition parameters (e.g laser power, gain, zoom factor,

resolution, and emission wavelengths reception), with detector settings optimized for low background and no pixel saturation. Pseudo-colored images were obtained using the “Red hot” look-up-table (LUT) of Fiji software (<http://www.fiji.sc/>).

TEM and cryo-EM

REM_{H6(86-198)} filaments were applied to previously glow-discharged carbon-coated copper 300 mesh grids and stained with a 2% uranyl acetate (w/v) solution. REM_{H6(86-198)} filaments were also prepared for cryo-EM. For the latter, lacey carbon copper grid were submitted to a standard glow discharge procedure and flash-frozen into a liquid ethane bath using EM GP (Leica). Specimens were observed under low-dose conditions using a cryo holder (Gatan, USA). Observations were performed with a FEI Tecnai F20 electron microscope operating at 200 KV and images were acquired using a digital 2k x 2k USC1000 camera (GATAN). Measurements of the repetitive patterns were calculated on FFT images of 10 selected areas. REM₍₈₆₋₁₉₈₎ filaments lacking the N-terminal His₆-tag were stained and applied to carbon-coated copper grids as described above. TEM images were recorded under low-dose conditions on a FEI CM120 120 kV FEI electron microscope using a Gatan USC1000 2k X 2k camera.

3D modelling

The 3D model of StREM1.3₍₁₁₇₋₁₆₆₎ was constructed by homology using the server I-TASSER (<https://zhanglab.ccmb.med.umich.edu/I-TASSER/>) (Zhang, 2008). Coiled-coil trimers were assembled using the SymmDock server (Schneidman-Duhovny et al., 2005) and a supplementary energy minimization step was performed with Yasara (<http://www.yasara.org/minimizationserver.htm>) (Krieger et al., 2009).

Solution NMR spectroscopy.

¹H,¹⁵N SOFAST-HMQC (band-Selective Optimized-Flip-Angle Short-Transient Heteronuclear Multiple-Quantum Correlation (Schanda et al., 2005)) experiment was carried out at 313 K on a protein sample containing 200 μM REM₍₈₆₋₁₉₈₎, 20 mM HEPES, 150 mM NaCl, 0.02% NaN₃, pH 7.4. Spectra were recorded on a Bruker Avance Neo 700 MHz spectrometer equipped with a 5 mm TXI 1H/13C/15N/2H

probe. The spectrum was acquired with 512 scans, 128 and 2048 complex points in F1 and F2 dimensions, respectively. Frequencies were calibrated according to DSS signal. The NMR data were processed using the TOPSPIN 4 software (Bruker Biospin).

Solid-state NMR spectroscopy

MAS solid-state NMR experiments were performed on a 600 MHz ($\text{REM}_{\text{H6}(86-198)}$) and 800 MHz ($\text{REM}_{(86-198)}$) ^1H Larmor frequency spectrometer (Bruker Biospin) using 3.2 mm MAS probes. Solid-state NMR rotors were filled with 10 mg of $\text{REM}_{\text{H6}(86-198)}$ or ($\text{REM}_{(86-198)}$) filaments and spun at 11 kHz for spectra acquisition. Sample temperature was set between 0-5°C according to DSS signal used as an internal reference (Bockmann et al., 2009). A ramped CP with a 1 ms ($\text{REM}_{\text{H6}(86-198)}$) and 0.7 ms ($\text{REM}_{(86-198)}$) contact time was used for the ^1H - ^{13}C cross-polarization (CP) transfer. An acquisition time of 20 ms and 2k scans were used for 1D ^1H - ^{13}C CP. For the 2D spectrum, the ^{13}C - ^{13}C polarization transfer was performed with proton-driven spin diffusion (PDS) applied for a mixing time of 50 ms to detect intra-residue correlations. Proton decoupling during the acquisition was achieved using a SPINAL-64 decoupling sequence (Fung et al., 2000). Acquisition times of 20 ms and 6.5 ms ($\text{REM}_{\text{H6}(86-198)}$), 20 ms and 7.5 ms ($\text{REM}_{(86-198)}$) were chosen for the direct and indirect dimensions, respectively. The total number of scans was 960 and 640 for a total experiment time of 6 and 7 days approximately, for $\text{REM}_{\text{H6}(86-198)}$ and $\text{REM}_{(86-198)}$ respectively. Secondary chemical shifts were calculated using random coil chemical shifts described by Wang and Jardetzky (Wang and Jardetzky, 2002). All data were processed using Topspin 3.2 (Bruker Biospin) and analyzed with CCPNMR Analysis software (Skinner et al., 2016). Backbone and sidechains ^{13}C chemical shifts were predicted from the protein 3D coordinates of the coiled-coil model spanning residues 117-166 using the software ShiftX2 (Han et al., 2011).

Results

REMORIN coiled-coil trimerization promoted by the highly-conserved C-terminal is essential for membrane targeting

REMORINs share a highly variable N-terminal domain in terms of length and conservation of the primary sequence and a highly conserved C-terminal region (Bariola et al., 2004; Raffaele et al., 2007; Reymond et al., 1996). Previous work on a *Solanum tuberosum* REMORIN of group 1 isoform 3 (StREM1.3) showed that the C-terminal region encompasses two distinct domains (Figure 1A): the short C-terminal anchor [171-198] (Perraki et al., 2012) specifically binds plasma membrane phosphatidylinositol 4-phosphate (PI4P) and mediates StREM1.3 PM nanodomain organization (Gronnier et al., 2017), while the region [86-170] contains a segment predicted to be implicated in the oligomerization of the protein (Bariola et al., 2004; Perraki et al., 2012). The latter domain displays a strong propensity to form a coiled-coil super helix (Figure 1B). In such structures, alpha helical monomers wind around each other to optimize protein-protein contacts and stabilize the multimer assembly (Crick, 1953; Kohn et al., 1997). All the members of the REMORIN family share these predicted structural properties and have strong sequence similarities between their C-terminal regions (Raffaele et al., 2007). We compared and analyzed the sequences of StREM1.3 with 5 *Arabidopsis thaliana* REMORINs from different groups (Groups 1, 3, 4, 5 and 6) to identify conserved elements that might be essential to the formation of coiled-coil super-helices (Figure 1B and S2). This comparison revealed a sequence similarity of 59 % with the most divergent, *i.e.* AtREM3.1, and 94% sequence similarity with AtREM1.3. Based on the chemical properties of the amino acids, we identified three candidates that could potentially be involved in the helix-helix interfaces within the coiled-coil domain (L126, L137 and L155). The hydrophobic character of the residues at these three positions is highly conserved between the different members of the REMORIN family. Figure 1C shows the coiled-coil helical wheel at position L155 for the StREM1.3 trimer. L152 and L155 form a hydrophobic patch, which stabilizes the coiled-coil structure. Polar and charged residues (H156, K157 and E158) are exposed either to the solvent or to an opposite charge residue, again potentially stabilizing the structure.

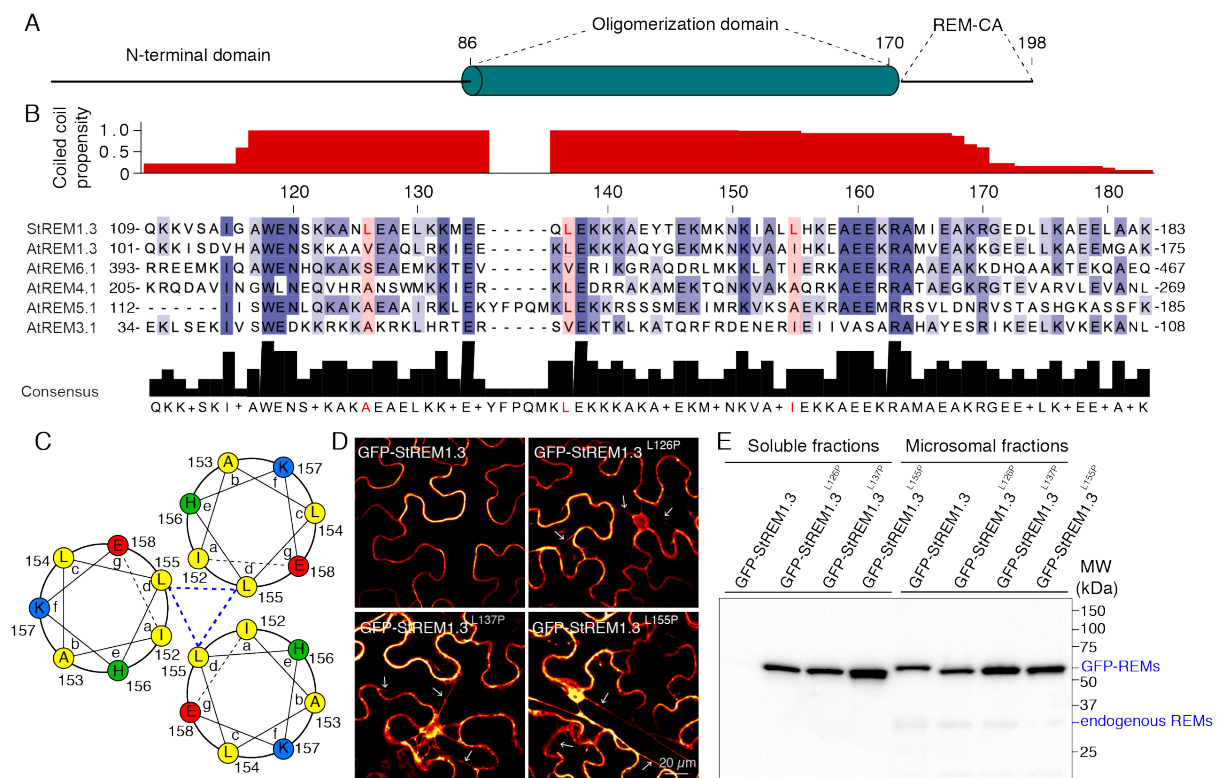


Figure 1. Mutations of conserved amino acid motifs in the coiled coil impairs PM targeting. (A) Domain organization in StRem1.3. (B) Coiled-coil propensity of StRem1.3 C-terminal region (109-183) realised with COILS. Sequence alignment of REMORIN homologs in *S. tuberosum* and *A. thaliana*. Protein sequences are ranked according to the conservation score. Hydrophobic residues potentially involved in helix contacts are highlighted in red. Conserved amino acids between the different REMORINs are shown in blue (dark blue for the most conserved to light blue for the less conserved). (C) Helical wheel corresponding to a coiled-coil trimer centred to the 152-158 region. Residues type are colored as follows: yellow, hydrophobic; blue, basic; red, acid; green, polar. Wheels were drawn using DrawCoil 1.0. (D) Confocal images presenting secant views of *N. benthamiana* epidermal cells expressing GFP-StREM1.3, GFP-StREM1.3^{L126P}, GFP-StREM1.3^{L137P}, GFP-StREM1.3^{L155P}, transiently expressed in tobacco epidermal cells. Scale bars: 20 μm. (E) Tobacco leaf cells expressing each construct were fractionated into soluble (sol.) and microsomal (m) compartments by centrifugation. Proteins were analyzed by Western blot with antibodies against StREM1.3. The protein loading control is presented in Figure S8.

We have recently reported structural insights into the role of the C-terminal peptide REM-CA during PM anchoring and nanodomain organization (Gronnier et al., 2017)

and we here aimed at testing the impact of StREM1.3 trimerization on its membrane-binding properties. Based on the sequence analyses, we introduced Prolines, in order to destabilize the coiled-coil superstructure (Chang et al., 1999), at positions L126, L137 and L155. *In vivo* confocal imaging visualized the subcellular localization of GFP-StREM1.3, GFP-StREM1.3^{L126P}, GFP-StREM1.3^{L137P} and GFP-StREM1.3^{L155P} (Figure 1D). As expected, the wild-type protein localized exclusively at the plasma membrane. However, for all mutants, fluorescence was detected in the cytosol, which indicates that the protein is no longer strictly associated with the plasma membrane. To further confirm this observation we performed cell fractionation of tissues expressing either GFP-StREM1.3, GFP-StREM1.3^{L126P}, GFP-StREM1.3^{L137P}, or GFP-StREM1.3^{L155P} (Figure 1E). Western blotting with anti-REM antibody (Raffaele et al., 2009) clearly confirmed that StREM1.3 is only found in the microsomal fraction whereas the three mutants are visible in both microsomal and soluble fractions. Altogether, these observations suggest that oligomerization might be required for REMORINs' PM localization.

Building blocks of assembled REM_{H6(86-198)} form organized fibers as revealed by TEM and cryo-EM

To investigate the assembly features and the structure of REMORIN oligomers, we focused on the conserved C-terminal region (residues 86 to 198), including the coiled-coil domain that most likely is responsible for the assembly (Bariola et al., 2004), and REMCA. We expressed and purified StREM1.3 C-terminal moiety (REM_{H6(86-198)}) in *E. coli*. After the purification, we recovered different fractions containing REM_{H6(86-198)} protein and analyzed them with gel-electrophoresis under denaturing conditions (Figure S1). The fractions containing pure REM_{H6(86-198)} were pooled and the self-assembly was triggered by dialysis. In order to provide an in-depth analysis of the mesoscopic shape as well as structural features of the assembly, we chose several biophysical techniques including negative staining transmission EM (TEM), cryo-EM and SSNMR. TEM and cryo-EM gave us first insights into the morphology of REM_{H6(86-198)} assemblies (Figure 2A and B, respectively), revealing ordered REMORIN fibers with a repetitive pattern. The repeating elements are propagated both horizontally and vertically. The periodicities

correspond to 13 nm along and approximately 5 nm perpendicular to the fiber axis. Interestingly, along the fibers, their width can vary (Figure S3) and their endings are irregular. The variable width engendering irregular endings of the fibers suggests an association and juxtaposition of thin filaments (arrow Figure 2C). This implies that the thin filaments self-assemble into large fibers in a constructive manner leading to the repetitive patterns.

Importantly, filaments of $REM_{(86-198)}$ without the N-terminal His₆-tag do not show specific lateral association (Figure 2D). However, the SSNMR data on $REM_{(86-198)}$ lacking the His₆-tag clearly confirm that the molecular structure of $REM_{(86-198)}$ in laterally associated ($REM_{H6(86-198)}$) and single filaments ($REM_{(86-198)}$) does not vary essentially, because the spectral fingerprint is conserved between both filaments (Figure S4). The lateral association of $REM_{H6(86-198)}$ filaments allows for the analysis of the repetitive patterns promoted by the His₆-tag, indicative of the assembly features.

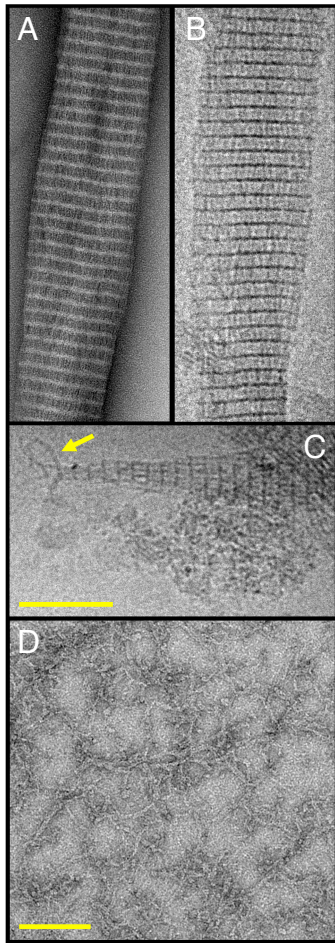


Figure 2. Electron micrographs of $REM_{H6(86-198)}$ and $REM_{(86-198)}$ filaments. (A) Negative staining TEM and (B) cryo-EM show filaments of $REM_{H6(86-198)}$ with two repetitive patterns perpendicular to each other. Width and thickness of fibers vary over the length of the filaments. (C) CryoEM of the sharp extremity of a $REM_{H6(86-198)}$ fiber shows similar repetitive motifs. Scale Bar of (A), (B) and (C) is the same: 100 nm (D) Negative-staining TEM micrograph of thin filaments of $REM_{(86-198)}$, lacking the N-terminal His6-tag. Scale Bar: 100 nm

The REMORIN coiled-coil domain gains a partially well-organized structure upon trimerization

To decipher the molecular basis underlying the filament formation, we performed a 3D modelling of the StREM1.3 coiled-coil domain based on sequence homology using the I-TASSER server (Zhang, 2008). The modelling was restrained to the region with the higher coiled-coil propensity [117-166] defined by the software COILS (Lupas et al., 1991). The 3D model converged to a regular alpha helix composed of

residues 133 to 166. REM₍₁₁₇₋₁₆₆₎ monomers were assembled into a trimer by geometry based docking using the SymmDock server (Schneidman-Duhovny et al., 2005). Figure 3A shows the trimeric coiled-coil structure of the REMORIN obtained *in silico*. A patch composed of hydrophobic residues, which point towards the trimer core, defines the interface between the three monomers and electrostatic interactions stabilize the architecture.

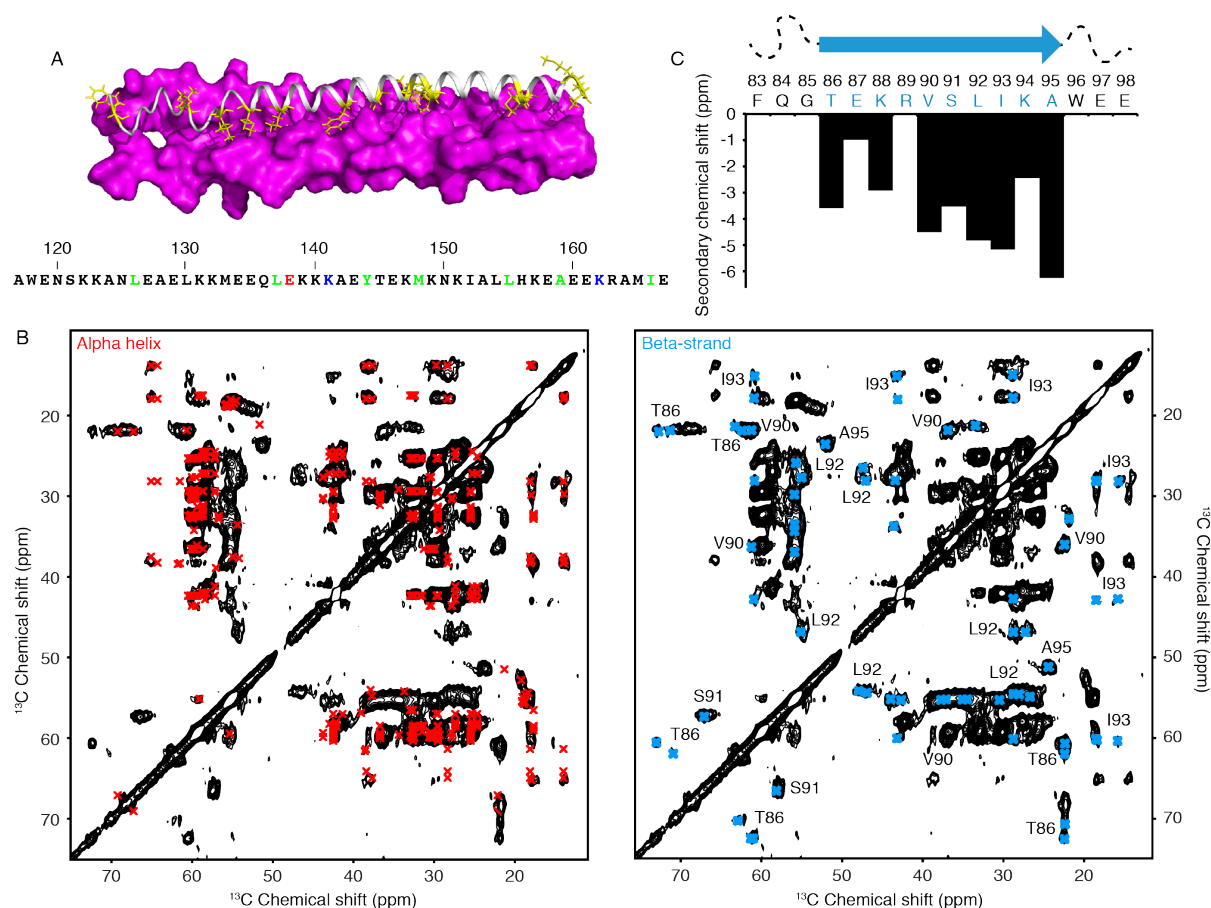


Figure 3. 3D model and solid-state NMR of REM_{H6(86-198)} filaments. (A) 3D model of StREM1.3 coiled coil domain predicted with I-TASSER server (Zhang, 2008). Two monomers in magenta are represented in surface mode and the third monomer with cartoon. All the hydrophobic side chains in the monomer are colored in yellow. Residue contacts identified between in StREM1.3 coiled-coil domain are highlighted on the primary sequence (green, hydrophobic contacts; red and blue, electrostatic contacts). (B) 2D PDSD ¹³C-¹³C spectrum of REM_{H6(86-198)} filaments (50 ms mixing time) showing back-calculated ¹³C chemical shifts with ShiftX2 from the 3D model (left spectrum, red crosses) and assigned chemical shift from β -strands (right spectrum, blue crosses). (C) Secondary chemical shift $\Delta\delta C_{\alpha}$ - $\Delta\delta C_{\beta}$ of the

T86-E87-K88-R89-V90-S91-L92-I93-K94-A95 amino acid segment in REM_{H6(86-198)}, revealing the presence of a β -strand segment.

SSNMR data on REM_{H6(86-198)} filaments support the 3D model of the coiled-coil domain and identify a short segment in β -strand conformation

To determine whether the 3D model obtained *in silico* reflects the structure adopted by REM_{H6(86-198)} in the filaments, we analyzed ¹⁵N,¹³C-labelled filaments using liquid and solid-state NMR. Solution NMR analysis revealed that REM_{H6(86-198)} is unstructured in solution and adopts a 3D fold only upon assembly into multimeric complexes (Figure S5). SSNMR is an emerging technique providing atomic structural information on molecular assemblies in their native states. We conceived a protocol to successfully produce, purify and assemble suitable quantities (~10mg) of ¹⁵N- and ¹³C-labelled REM_{H6(86-198)} *in vitro* to conduct multidimensional MAS SSNMR on the REMORIN in its filamentous state. The very intense signal observed in a one-dimensional ¹H-¹³C cross-polarization spectrum revealed the presence of a rigid core in the structure of the assembled proteins (Figure S6). A two-dimensional ¹³C-¹³C PDSD (proton-driven spin diffusion), Figure 3B, acquired with a short mixing time (50ms) set up to detect intra-residues ¹³C-¹³C correlations, reveals the SSNMR fingerprint of the REM_{H6(86-198)} structure in filaments. The intense signals again indicate that the filaments contain a rigid protein core and the appearance of well-resolved individual peaks points to a well-defined atomic structure adopted by the monomers composing the assembly. Our *in silico* 3D model of REM₍₁₁₇₋₁₆₆₎ suggests that the REMORIN monomers oligomerize into α -helical coiled-coil trimers promoted by the coiled-coil domain. Based on the 3D model, we used the ShiftX2 software (Han et al., 2011) to predict the expected protein ¹³C chemical shifts for the coiled-coil domain REM₍₁₁₇₋₁₆₆₎ and reported them on the 2D ¹³C-¹³C SSNMR spectrum recorded on REM_{H6(86-198)} filaments (Figure 3B, red crosses, left spectrum). The majority of the predicted chemical shifts match well with the experimentally observed signals. This strongly supports the model of a α -helical tertiary fold in the filament core, reflecting the coiled-coil domain. However, a non-negligible part of the signals in the 2D spectrum remain unassigned and do not appear in spectral regions where

signals from α -helical structural segments are located (Figure 3B, blue crosses, right spectrum). Among them, a detailed analysis was possible for Thr, Glu, Lys, Val, Ser, Leu, Ile, and Ala amino acids for which the resonances reflecting β -strand secondary structures are isolated in the spectrum. By comparing these residue-specifically assigned amino acids with the primary sequence of REM_{H6(86-198)} we identified the unique motif in the REM_{H6(86-198)} primary sequence (T₈₆-EKRVSLIKA-A₉₅) adjacent to the coiled-coil region. The theoretical sequential peaks are all visible even if their assignments remain ambiguous. The local conformation of these residues was identified via their secondary chemical shifts that reflect a β -strand conformation where negative values were obtained. The unique amino acid composition of T₈₆-EKRVSLIKA-A₉₅ and the clear β -strand conformation of the identified residues indicate the occurrence of a short β -segment at this location (Figure 3D). The assignment of the R89 spin system remained ambiguous because of the important peak overlap in this spectral region. Likewise, the region around T₈₆-A₉₅ region might be extended but the chemical shifts of these residues could not be identified due to spectral overlap.

Cryo-EM data suggest that trimeric coiled-coil REM_{H6(86-198)} arranges itself as aligned building blocks into filaments

Cryo-EM micrographs revealed the repetitive motifs in the REM_{H6(86-198)} filaments and the spectral resolution we obtained on the filaments allowed for the detailed measurement of their dimensions (Figure 4A). The longitudinal repetitions are characterized by 13 nm in length with a width of approximately 5 nm. The dimensions of the 3D model of the REM₍₁₁₇₋₁₆₆₎ coiled-coil trimer, with 8 nm in length and a width of \sim 1.5 nm without side-chains (Figure 4A), tie in the distances obtained on the electron micrograph of the REM_{H6(86-198)} fibers. The 3D model of the coiled-coil domain illustrates the tertiary fold of the REM₍₁₁₇₋₁₆₆₎ with the region spanning 132-166 showing well-defined α -helices, slightly twisted to allow protein-protein contacts at positions 155 and 137 (Figure 4A, B). The segment 117-131 is less ordered than expected for the coiled-coil domain but displays lower structure accuracy for the generated model (Figure S7). Figure 4B shows an example of close hydrophobic

contacts between Leucine residues in the trimer at the position 155, essential for trimer stability.

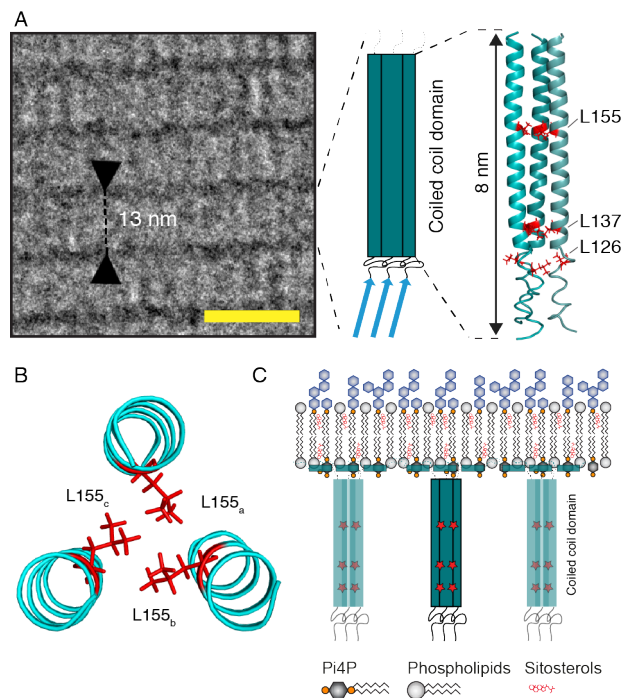


Figure 4. 3D architecture of $REM_{(86-198)}$ inside the filaments and associated to PM nanodomains. (A) Cryo-EM micrograph of $REM_{H6(86-198)}$ fibers depicts 13 nm horizontal repetitive patterns corresponding to a regular assembly of $REM_{H6(86-198)}$. Scale bar: 20nm. Schematic representation of $REM_{H6(86-198)}$ structure inside the filament (β -strands are represented as blue arrows and α -helices as rectangles) and 3D structural model of $REM_{(86-198)}$ coiled-coil domain. (B) Example of protein contacts inside the coiled coil domain. α -helices are represented in cartoon and Leucine sidechains in sticks. (C) Schematic representation of $REM_{(86-198)}$ structure when associated to the PM nanodomains. Red stars represent point mutations, which impair the membrane localization of StREM1.3. α -helices are represented as rectangles. The C-terminal membrane anchor REM-CA contains a short α -helix. Point mutations for *in vivo* confocal imaging experiments are highlighted in red.

Based on the ensemble of our results we propose a cartoon model of the $REM_{H6(86-198)}$ building block in filaments, encompassing a coiled-coil domain, in which the three membrane-affinity impairing mutations are localized, flanked by a short β -strand and supposedly two segments with less well-defined structures on both sides (Figure 4A).

The N-terminal ending of the coiled-coil domain contains a region of less defined structure and a stretch of 10 amino acids, mainly composed of hydrophobic residues constituting a regular β -strand, whereas the C-terminal REM-CA seems to adopt a condensed, unstructured form. The two endings account for the regions of dense protein concentration in the EM micrographs. The proximity of the β -strands could stabilize the trimer through an inter-strand hydrogen-bonding network.

Discussion and Conclusion

Our results have demonstrated an unexpected impact of REMORIN oligomerization via the coiled-coil domain on membrane affinity and we therefore decided to tackle the structure of this best-characterized nanodomain-associated plant protein supramolecular assembly.

By using a coiled-coil prediction server, we identified the region with the highest propensity of forming a coiled-coil and we singled out three hydrophobic residues that could stabilize the trimeric architecture, L126, L137 and L155. *In vivo* monitoring of the localization of REMORIN and of the three substitution mutants by confocal microscopy showed that all three mutations strongly impair membrane affinity suggesting that trimer formation is correlated with REMORIN-membrane interactions and that a cooperative effect between REMORINs plays an important role in membrane binding.

Full-length REMORINs form filaments, which were proposed to arise from interactions between coiled-coil trimers of the conserved C-terminal region (Bariola et al., 2004). We show that REM₍₈₆₋₁₉₈₎, lacking the highly variable N-terminal region, also assembles into well-organized filaments. When the N-terminal His₆-tag of REM₍₈₆₋₁₉₈₎ is conserved, i.e. REM_{H6(86-198)}, the filaments arrange into fibers that vary in width over the filament length and end in a thin architecture. This behaviour is consistent with the association or dissociation of trimeric building blocks that build a strong intermolecular network of weak interactions. Importantly, these fibers show very homogeneous repetitive patterns in electron micrographs that enable the analysis of the molecular building blocks in the filaments.

Creating an *in silico* 3D model of the coiled-coil domain allowed us to visualize the underlying 3D structures, to identify stabilizing hydrophobic and electrostatic contacts

and to estimate the dimensions of such coiled-coil trimer. In this model, the three Leucines are located in essential positions, explaining the destabilizing effect and membrane-affinity loss of Proline mutations, L126P, L137P and L155P.

To corroborate our working model of trimeric coiled-coil building units, we performed SSNMR on REM_{H6(86-198)} and REM₍₈₆₋₁₉₈₎ filaments, obtaining atomic structural data on the intact filaments. Based on the 3D trimeric model, we compared predicted with observed SSNMR chemical shifts, validating the hypothesis of trimeric coiled-coil units that associate laterally and, furthermore, residue-type and sequential assignments revealed longitudinal interactions between the trimers involving a short β -strand and less well-ordered condensed segments. The dimensions of the building blocks obtained from cryo-EM micrographs are compatible with the trimeric REM_{H6(86-198)} coiled-coil units, derived from the 3D model. Combining the structural data from SSNMR, the *in silico* model, and cryo-EM, we propose a cartoon model that reflects the architecture in REM_{H6(86-198)} and REM₍₈₆₋₁₉₈₎ filaments (Figure 4A). Furthermore, incorporating the recently proposed model of the REM-CA peptide structure during nanodomain formation and the data obtained on the role and structure of coiled-coil trimers, we propose a cartoon model for the nanodomain-associated REM₍₈₆₋₁₉₈₎ (Figure 4C). The coiled-coil trimers are stabilized by intermolecular protein-protein interactions including the three Leucine-Leucine contacts of residues 126, 137 and 155 (Figure 4C, red stars).

Conclusions

Protein organization into membrane domains relies on complex and scarcely in-detail explored structural mechanisms, involving lipid-protein and protein-protein interactions (Simons and Sampaio, 2011). Considered as genuine PM nanodomain-organized proteins in plants, REMORINs attach to the PM and concentrate in nanodomains by an original mechanism via the C-terminal anchor, REM-CA (Gronnier et al., 2017). We here report that REM-CA alone is not sufficient and responsible for membrane targeting. We show that the conserved trimerization region plays a central role and we investigated the structure of this region by conceiving a protocol to obtain filaments of mesoscopic scale that we analyzed by various

techniques. The obtained data and proposed cartoon model might also reveal other modes of interaction of REMORINs during oligomerization such as β -strand hydrogen bonding. However, the interactions between trimer coiled-coil domains promoting the filament assembly might reflect interactions that favour the highly specific nanoclustering occurring between REMORINs of the same family (Jarsch et al., 2014). Our findings open an avenue to understanding the complex nanodomain-targeting mechanisms of REMORIN proteins based on the combination of SSNMR and cryo-EM and aim at contributing to the comprehension of molecular strategies employed by membrane-domain proteins to perform their cellular functions.

Acknowledgments

We acknowledge the financial support by the ANR (ANR-13-PDOC-0017-01 to B.H. and ANR-14-CE09-0020-01 to A.L.), the IdEx Bordeaux "Investments for the future" (ANR-10-IDEX-03-02 to B.H.) and PEPS to B.H. and S.M., the European Research Council (ERC-2015-StG GA no. 639020 to A.L.) and the CNRS (IR-RMN FR3050). A.L. is supported by the Ministère de l'Enseignement Supérieur et de la Recherche, France (MERS, doctoral grants). TEV protease was a gift from Lionel Beaurepaire and the work has benefited from the facilities and expertise of the Biophysical and Structural Chemistry platform (BPCS) at IECB, CNRS UMS3033, Inserm US001, Bordeaux University <http://www.iecb.u-bordeaux.fr/index.php/fr/plateformestecnologiques> »

References

- Bai, X.C., McMullan, G., Scheres, S.H., 2015. How cryo-EM is revolutionizing structural biology. *Trends in biochemical sciences* 40, 49-57.
- Bariola, P.A., Retelska, D., Stasiak, A., Kammerer, R.A., Fleming, A., Hijri, M., Frank, S., Farmer, E.E., 2004. Remorins form a novel family of coiled coil-forming oligomeric and filamentous proteins associated with apical, vascular and embryonic tissues in plants. *Plant Mol Biol* 55, 579-594.
- Bockmann, A., Gardiennet, C., Verel, R., Hunkeler, A., Loquet, A., Pintacuda, G., Emsley, L., Meier, B.H., Lesage, A., 2009. Characterization of different water pools in solid-state NMR protein samples. *Journal of biomolecular NMR* 45, 319-327.
- Bucherl, C.A., Jarsch, I.K., Schudoma, C., Segonzac, C., Mbengue, M., Robatzek, S., MacLean, D., Ott, T., Zipfel, C., 2017. Plant immune and growth receptors share common signalling components but localise to distinct plasma membrane nanodomains. *Elife* 6.
- Chang, D.K., Cheng, S.F., Trivedi, V.D., Lin, K.L., 1999. Proline affects oligomerization of a coiled coil by inducing a kink in a long helix. *J Struct Biol* 128, 270-279.
- Crick, F.H., 1953. The packing of $[\alpha]$ -helices: simple coiled-coils. *Acta Cryst.* 6, 689-697.

- Earl, L.A., Falconieri, V., Milne, J.L., Subramaniam, S., 2017. Cryo-EM: beyond the microscope. *Curr Opin Struct Biol* 46, 71-78.
- Edgar, R.C., 2004. MUSCLE: multiple sequence alignment with high accuracy and high throughput. *Nucleic Acids Res* 32, 1792-1797.
- Fung, B.M., Khitritin, A.K., Ermolaev, K., 2000. An improved broadband decoupling sequence for liquid crystals and solids. *Journal of magnetic resonance* 142, 97-101.
- Grecco, H.E., Schmick, M., Bastiaens, P.I., 2011. Signaling from the living plasma membrane. *Cell* 144, 897-909.
- Gronnier, J., Crowet, J.M., Habenstein, B., Nasir, M.N., Bayle, V., Hosy, E., Platre, M.P., Gouguet, P., Raffaele, S., Martinez, D., Grelard, A., Loquet, A., Simon-Plas, F., Gerbeau-Pissot, P., Der, C., Bayer, E.M., Jaillais, Y., Deleu, M., Germain, V., Lins, L., Mongrand, S., 2017. Structural basis for plant plasma membrane protein dynamics and organization into functional nanodomains. *Elife* 6.
- Gui, J., Liu, C., Shen, J., Li, L., 2014. Grain setting defect1, encoding a remorin protein, affects the grain setting in rice through regulating plasmodesmatal conductance. *Plant Physiol* 166, 1463-1478.
- Habenstein, B., Loquet, A., 2015. Solid-state NMR: An emerging technique in structural biology of self-assemblies. *Biophys Chem*.
- Han, B., Liu, Y., Ginzinger, S.W., Wishart, D.S., 2011. SHIFTX2: significantly improved protein chemical shift prediction. *Journal of biomolecular NMR* 50, 43-57.
- Jarsch, I.K., Ott, T., 2011. Perspectives on remorin proteins, membrane rafts, and their role during plant-microbe interactions. *Mol Plant Microbe Interact* 24, 7-12.
- Jarsch, I.K., Konrad, S.S., Stratil, T.F., Urbanus, S.L., Szymanski, W., Braun, P., Braun, K.H., Ott, T., 2014. Plasma Membranes Are Subcompartmentalized into a Plethora of Coexisting and Diverse Microdomains in Arabidopsis and Nicotiana benthamiana. *Plant Cell* 26, 1698-1711.
- Jiang, W., Tang, L., 2017. Atomic cryo-EM structures of viruses. *Curr Opin Struct Biol* 46, 122-129.
- Kasai, R.S., Kusumi, A., 2014. Single-molecule imaging revealed dynamic GPCR dimerization. *Curr Opin Cell Biol* 27, 78-86.
- Kohn, W.D., Mant, C.T., Hodges, R.S., 1997. Alpha-helical protein assembly motifs. *The Journal of biological chemistry* 272, 2583-2586.
- Krieger, E., Joo, K., Lee, J., Lee, J., Raman, S., Thompson, J., Tyka, M., Baker, D., Karplus, K., 2009. Improving physical realism, stereochemistry, and side-chain accuracy in homology modeling: Four approaches that performed well in CASP8. *Proteins* 77 Suppl 9, 114-122.
- Lefebvre, B., Timmers, T., Mbengue, M., Moreau, S., Herve, C., Toth, K., Bittencourt-Silvestre, J., Klaus, D., Deslandes, L., Godiard, L., Murray, J.D., Udvardi, M.K., Raffaele, S., Mongrand, S., Cullimore, J., Gamas, P., Niebel, A., Ott, T., 2010. A remorin protein interacts with symbiotic receptors and regulates bacterial infection. *Proceedings of the National Academy of Sciences of the United States of America* 107, 2343-2348.
- Lingwood, D., Simons, K., 2010. Lipid rafts as a membrane-organizing principle. *Science* 327, 46-50.
- Loquet, A., Habenstein, B., Lange, A., 2013. Structural investigations of molecular machines by solid-state NMR. *Accounts of chemical research* 46, 2070-2079.
- Lupas, A., Van Dyke, M., Stock, J., 1991. Predicting coiled coils from protein sequences. *Science* 252, 1162-1164.
- Lupas, A.N., Bassler, J., 2017. Coiled Coils - A Model System for the 21st Century. *Trends in biochemical sciences* 42, 130-140.
- Marin, M., Thallmair, V., Ott, T., 2012. The intrinsically disordered N-terminal region of AtREM1.3 remorin protein mediates protein-protein interactions. *The Journal of biological chemistry* 287, 39982-39991.

- McBride, Z., Chen, D., Reick, C., Xie, J., Szymanski, D.B., 2017. Global analysis of membrane-associated protein oligomerization using protein correlation profiling. *Mol Cell Proteomics*.
- Meier, B.H., Bockmann, A., 2015. The structure of fibrils from 'misfolded' proteins. *Curr Opin Struct Biol* 30, 43-49.
- Perraki, A., Cacas, J.L., Crowet, J.M., Lins, L., Castroviejo, M., German-Retana, S., Mongrand, S., Raffaele, S., 2012. Plasma membrane localization of *Solanum tuberosum* remorin from group 1, homolog 3 is mediated by conformational changes in a novel C-terminal anchor and required for the restriction of potato virus X movement]. *Plant Physiol* 160, 624-637.
- Raffaele, S., Mongrand, S., Gamas, P., Niebel, A., Ott, T., 2007. Genome-wide annotation of remorins, a plant-specific protein family: evolutionary and functional perspectives. *Plant Physiol* 145, 593-600.
- Raffaele, S., Bayer, E., Lafarge, D., Cluzet, S., German Retana, S., Boubekour, T., Leborgne-Castel, N., Carde, J.P., Lherminier, J., Noirrot, E., Satiat-Jeunemaitre, B., Laroche-Traineau, J., Moreau, P., Ott, T., Maule, A.J., Reymond, P., Simon-Plas, F., Farmer, E.E., Bessoule, J.J., Mongrand, S., 2009. Remorin, a solanaceae protein resident in membrane rafts and plasmodesmata, impairs potato virus X movement. *Plant Cell* 21, 1541-1555.
- Reymond, P., Kunz, B., Paul-Pletzer, K., Grimm, R., Eckerskorn, C., Farmer, E.E., 1996. Cloning of a cDNA encoding a plasma membrane-associated, uronide binding phosphoprotein with physical properties similar to viral movement proteins. *Plant Cell* 8, 2265-2276.
- Schanda, P., Kupce, E., Brutscher, B., 2005. SOFAST-HMQC experiments for recording two-dimensional heteronuclear correlation spectra of proteins within a few seconds. *Journal of biomolecular NMR* 33, 199-211.
- Schneidman-Duhovny, D., Inbar, Y., Nussinov, R., Wolfson, H.J., 2005. PatchDock and SymmDock: servers for rigid and symmetric docking. *Nucleic Acids Res* 33, W363-367.
- Simons, K., Sampaio, J.L., 2011. Membrane organization and lipid rafts. *Cold Spring Harb Perspect Biol* 3, a004697.
- Skinner, S.P., Fogh, R.H., Boucher, W., Ragan, T.J., Mureddu, L.G., Vuister, G.W., 2016. CcpNmr AnalysisAssign: a flexible platform for integrated NMR analysis. *Journal of biomolecular NMR* 66, 111-124.
- Suzuki, K.G., Kasai, R.S., Hirosawa, K.M., Nemoto, Y.L., Ishibashi, M., Miwa, Y., Fujiwara, T.K., Kusumi, A., 2012. Transient GPI-anchored protein homodimers are units for raft organization and function. *Nat Chem Biol* 8, 774-783.
- Toth, K., Stratil, T.F., Madsen, E.B., Ye, J., Popp, C., Antolin-Llovera, M., Grossmann, C., Jensen, O.N., Schussler, A., Parniske, M., Ott, T., 2012. Functional domain analysis of the Remorin protein LjSYMREM1 in *Lotus japonicus*. *PloS one* 7, e30817.
- Troshin, P.V., Procter, J.B., Barton, G.J., 2011. Java bioinformatics analysis web services for multiple sequence alignment--JABAWS:MSA. *Bioinformatics* 27, 2001-2002.
- Tycko, R., Wickner, R.B., 2013. Molecular structures of amyloid and prion fibrils: consensus versus controversy. *Accounts of chemical research* 46, 1487-1496.
- Vonck, J., Mills, D.J., 2017. Advances in high-resolution cryo-EM of oligomeric enzymes. *Curr Opin Struct Biol* 46, 48-54.
- Wang, Y., Jardetzky, O., 2002. Probability-based protein secondary structure identification using combined NMR chemical-shift data. *Protein science : a publication of the Protein Society* 11, 852-861.
- Waterhouse, A.M., Procter, J.B., Martin, D.M., Clamp, M., Barton, G.J., 2009. Jalview Version 2--a multiple sequence alignment editor and analysis workbench. *Bioinformatics* 25, 1189-1191.

Weingarth, M., Baldus, M., 2013. Solid-state NMR-based approaches for supramolecular structure elucidation. *Accounts of chemical research* 46, 2037-2046.

Zhang, Y., 2008. I-TASSER server for protein 3D structure prediction. *BMC Bioinformatics* 9, 40.